

Evaluating the Performance of Novel TPMS-Based Acoustic Liner Designs Suitable for Additive Manufacturing

**Alden Packer¹, C. Aaron Reimann², Julian Winkler², Kenji Homma², Jeffrey Mendoza²,
Eric Greenwood³, Michael Manahan^{1,4}, Nicholas Meisel^{5,*}**

* Corresponding Author: nam20@psu.edu

¹ Department of Mechanical Engineering, The Pennsylvania State University, University Park,
PA 16802

² RTX Technology Research Center, East Hartford, CT 06108

³ Department of Aerospace Engineering, The Pennsylvania State University, University
Park, Pa 16802

⁴ Penn State Applied Research Laboratory, State College, PA 16801

⁵ School of Engineering Design and Innovation, The Pennsylvania State University, University
Park, PA 16802

Abstract

Acoustic liners are integral to the noise management of aircraft engines. As such, acoustic liner designs and configurations are the subject of research and development to address the acoustic requirements of next generation engine layouts. Perforate sheet over honeycomb core, or single degree of freedom (SDOF) liners and double degree of freedom (DDOF) liners are traditional designs that have been used in turbofan engines for many years to reduce noise. Leveraging the design freedom of additive manufacturing, our current research explores the use of triply periodic minimal surface (TPMS) lattices as an advanced core structure for acoustic liners. In this study, previously developed design exploration methods are applied to identify and compare the performance of novel TPMS acoustic liners to SDOF and DDOF liners. The comparisons are used to assess the viability of TPMS-based novel acoustic liner designs and justify the need to further explore through future research efforts.

1. Introduction and Motivation

Acoustic liners are standard treatment in the walls of aircraft nacelles (see Figure 1a) where they reduce the noise that is produced by the fan and other engine components. With advancements in modern aircraft designs that have led to more efficient, high-bypass ratio engines, research into more efficient and effective acoustic liners is required to address changes in the noise profile of new engine concepts. High bypass ratio engines have a noise profile that is much more fan-driven than older designs where the noise profile was largely produced by the jet [1,2]. Because the fan of high-bypass ratio engines produce lower frequency noise signatures, associated with the fan blade pass frequency, novel acoustic liners must achieve good acoustic absorption over a large frequency band. One of the most basic acoustic liner constructions is the single degree of freedom (SDOF) acoustic liner, which consists of a rigid backplate, honeycomb core, and perforated facesheet, as shown in Figure 1b. This type of acoustic liner is one of the current designs implemented in aircraft engines and places the perforated facesheet oriented so that it faces the sound-producing components. The SDOF acoustic liner is limited in its design, which is primarily based on the facesheet perforations and the depth of the honeycomb core. The liner depth for a SDOF acoustic liner is related to the absorbed frequencies, with deeper cores attenuating the longer

wavelengths of low frequency noise. The second liner type that is currently in use is a variation of the SDOF, and is referred to as a double degree of freedom (DDOF) liner, where a perforated septum cuts through the honeycomb core [3]. DDOF acoustic liners have the potential for wider bandwidths of acoustic absorption, for the same footprint, typically allowing for additional acoustic absorption at higher frequencies than SDOF liners of the same thickness.

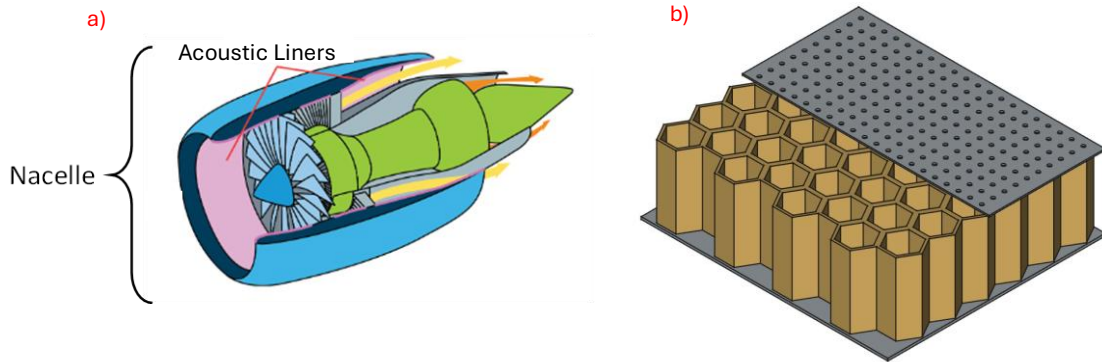


Figure 1. a) Acoustic liner treatments (shown in pink) line the inner surface of the aircraft nacelle (adapted from Ref. [1]) and b) Traditional acoustic liners consist of a rigid backplate, honeycomb core, and perforated facesheet.

While SDOF and DDOF liners are the more standard designs used in industry today, novel acoustic liner concepts are being explored to achieve lower frequency absorption and increase the overall acoustic absorption in the nacelle. Additive manufacturing (AM) has brought design freedom to this exploration process to allow for novel geometries that would not have been previously manufacturable. NASA has proposed several honeycomb and concepts that contain channels of varying length covered by facesheets [1,3,4]. AM has enabled rapid prototyping of these novel concepts. Similarly, ONERA explored other AM enabled liner concepts that contain complex internal channels, irregularly shaped inlets, and stacked patterns [4]. In addition, triply periodic minimal surface (TPMS) lattices are complex structures that are gaining attention, as they are now manufacturable through AM. While they contain many of the same benefits of other lattice structures, such as high strength to weight ratios, they have also been observed to have unique acoustic behaviors [5]. With the modeling and manufacturing tools now available, it is possible to explore the potential of TPMS lattice-based acoustic liners. However, to show the viability of these novel acoustic liner designs, a comparison with the traditional, currently implemented, acoustic liners is required.

In this paper, we compare the performance of optimized TPMS acoustic liners with optimized traditional liners, the SDOF and DDOF. All liners are optimized using the same absorption targets and the results are compared. Section 2 will present additional background information about modern acoustic liners, the design and modeling of modern acoustic liners, and TPMS lattice structures as candidates for acoustic liner applications. Section 3 will then outline the design and optimization process used to compare TPMS-based liners with traditional liners and explore the design variables and modeling techniques of each. In Section 4, the results for the optimization process of each liner will be reported and discussed, and the performance of the TPMS-based liners will be compared to traditional liners.

2. Background

To provide context for this study, it is necessary to review the construction and function of traditional liners in more detail and to identify the role that AM has played in acoustic liner development. The presence of AM-enabled TPMS lattices in the field of acoustics will then be reviewed. Finally, the various levels of fidelity required to model the acoustic performance across liners, both simple and complex, will be discussed.

2.1. Traditional Acoustic Liners

Honeycomb sandwich panels are common structures in the composites and aerospace industries due to their rigidity and lightweight construction. The honeycomb core has sufficient compressive strength to resist buckling with the bulk of the load being carried in the top and bottom of the structure. SDOF and DDOF acoustic liners are created from these types of structures. Structurally, these types of liners are capable of withstanding the loads required for placement within a turbofan engine nacelle. Acoustically, the cavities within each honeycomb cell structure works in conjunction with an added perforated facesheet to create a mass-spring system that absorbs incoming sound energy, based on the principles of Helmholtz resonators [6]. In design of the SDOF and DDOF acoustic liners, the depth of the liner, the perforation hole size, and the hole distribution are adjusted to achieve acoustic absorption at a target frequency or frequency range [7].

While SDOF and DDOF liners have been used in aircraft engines for many years, there is ongoing research to improve liner designs, to increase the broadband capacity of the liners, and to allow them to attenuate lower frequency noise. One such design is the multi-degree of freedom (MDOF) liner concept. Similar to the DDOF liner concept, which has a single perforated septum located at a fixed location or constant depth within all the cells in the honeycomb core, the MDOF liner concept has more than one septum placed at various depths within the adjacent cells in the honeycomb core [3]. Other novel acoustic liner concepts involve straight channels of varied depth, each tuned to attenuate a specific frequency [4,7,8]. To allow for a wider range of frequency tuning, the concept of straight channels with bends that snake through a structure has been explored using the rapid prototyping capabilities of AM [4,9].

2.2. Advanced Liner Concepts Enabled by AM

AM has impacted the development of novel acoustic liners; even those based on honeycomb cores can be explored and experimentally tested before committing to a final manufacturing process [10,11]. Design freedom is another benefit of AM that is exploited, with studies looking into the cross-sectional shape of a resonating channel or using spiral channels [4]. Controlling the path of the air within an acoustic liner is an objective for many of these studies [4,9,12]. AM has also enabled other complex structures, such as lattice structures, to be implemented in sound transmission and absorption applications [13–15].

TPMS lattices are a family of lattice structures known for their complex yet smooth and continuous geometry. TPMS lattices are defined mathematically through equations that control important design variables such as wall thickness, unit cell size, and volume fraction.

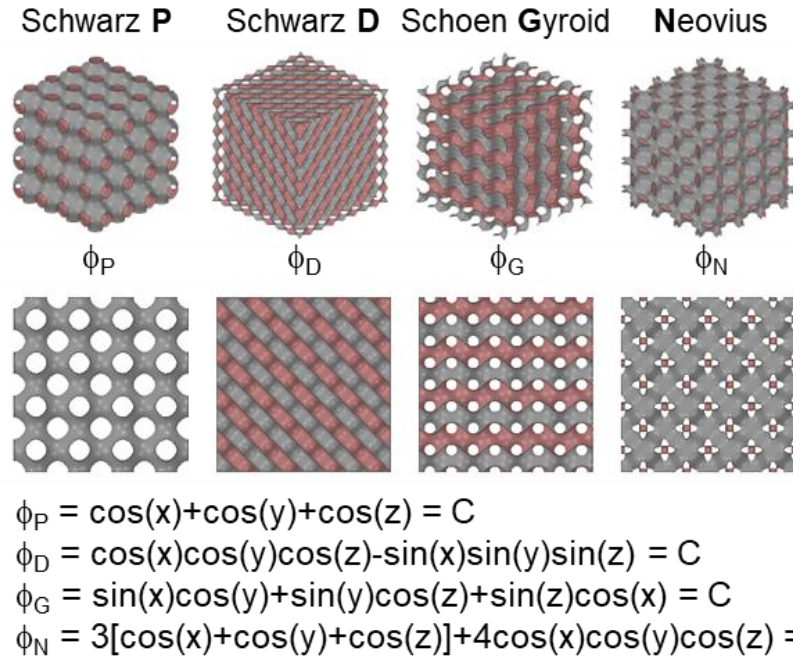


Figure 2. Examples of TPMS lattice geometries, with the defining equations of each.

These lattices have become much more common due to the ability of leveraging AM to fabricate them, as well as implicit geometry modeling software that can efficiently model them [16]. Like strut-based lattice structures, TPMS lattices exhibit high strength to weight ratios and energy absorbing characteristics, making them excellent candidates for parts and systems requiring light-weighting or structural damping [17–19]. The continuous, flowing channels of TPMS structures have also been leveraged in the field of heat transfer, where TPMS lattice-based heat exchangers have been explored [20–22]. Investigations in heat transfer and fluid flow of TPMS lattices was often performed with the goal of characterizing physical behaviors, such as pressure drop or heat transfer coefficient according to the lattice design variables such as wall thickness and porosity [22,23].

AM lattice structures have also been explored for use in the field of acoustics, particularly in sound transmission loss applications, because of their ability to reduce the propagation of elastic waves [13,24–28]. TPMS lattices have been explored for acoustic potential as well, [24,29–31]. Beneficially, the controllable tortuosity of TPMS lattices allows for the control of the structure’s air flow resistivity [23]. Their unique repeating structures also create an opportunity to harness natural frequency bandgaps created by the geometry [5,14,28]. The addition of a facesheet onto a lattice structure backing was explored in [15]; however the exploration of liner designs that consist of a TPMS lattice with a facesheet has been limited, with [2] showing the result of adding a facesheet to a uniform Schwarz P TPMS structure. Through manipulation of the TPMS lattice defining equations, as shown in Figure 2, these structures can be customized to achieve a tailored acoustic response. Using different TPMS lattice types and altering controllable factors in conjunction with a perforated facesheet has yet to be explored.

2.3. Acoustic Performance Prediction

The performance of acoustic liners is predictable through several methods, which are based on a range of fidelity. The use of one method over another comes down to how complex the geometry is of the liner being modeled, the required model fidelity to capture the necessary physics, and the available software and computational resources. Analytical models provide the lowest computational cost and are the most efficient to solve, though the fidelity of these models is lower than other methods [32–35]. The lumped element, or two-parameter, model (see [36]) and the Zwikker-Kosten transmission line (ZKTL) model (see [7,37]) are two analytical methods for predicting acoustic liner performance. Mid-fidelity solvers are finite element (FE) based methods that are used to predict acoustic liner performance by explicitly modeling the geometries [2,38,39]. High-fidelity models also use finite element methods, however, they use a much finer mesh and resolve the thermal fluid boundary layer to capture the thermoviscous acoustic effects [2,40–42]. The high-fidelity models require much more computational resources as compared to the analytical or mid-fidelity models, but the results capture a more complete picture of the physics acting in the acoustic liner.

For traditional liners, acoustic performance can be predicted using low-fidelity analytical models. Even some of the novel, AM-enabled liner designs that make use of straight channels can be modeled using analytical methods. However, for more complex geometries, like TPMS lattices, analytical tools are not available to predict performance. In these cases, mid-fidelity solvers are required. By using a combination of analytical models for predicting the traditional liner performance, and an FE solver for predicting TPMS liner performance, both types of liners can be optimized and their acoustic performance can be compared.

3. Optimization Process

To verify the viability of TPMS lattice-based acoustic liners, a comparison is made against traditional SDOF and DDOF liners. Both categories of liners were first optimized using the same target objectives, that of maximizing acoustic absorption in defined frequency ranges. The design optimization process that was used was created through the unification of necessary pieces of software that performed the functions of parameterizing the design variables for the acoustic liner concepts, modeling the geometries, simulating the acoustics physics, and analyzing the response objectives.

3.1. Parameterization of the Design Variables

For SDOF, DDOF, and TPMS based liners alike, optimization requires that the available design variables be parameterized and given bounds within which to explore. For each liner type, and subsequent construction, there are changes to the design that can impact the acoustic performance of the liner. This subsection outlines what those design variables are for each liner type. For all liner types, the total depth or thickness of the liner was capped at 1.5” or 38.1 mm, to compare the performances of the lattices when similarly constrained. The design variables of the facesheet were also given equal constraints across all linertypes.

3.1.1. SDOF and DDOF Acoustic Liners

For this investigation, the SDOF acoustic liner has four main design variables, shown in Figure 3a. Three of the variables correspond to properties of the perforated facesheet, percent open area (POA), facesheet thickness, t , and perforation diameter, d . To eliminate the possibility

of the POA and perforation diameter requiring a non-whole number of perforations, the number of perforations was used as a design variable, and the POA was calculated from the number of perforations multiplied by the area of a single perforation, all divided by the total area of a cell. That POA value was then used in modeling. The facesheet variables affect the acoustic response by creating resistive losses through friction in the perforations. The depth of the honeycomb core, D , is a critical variable for resonating liners, like the SDOF. Varying the depth of the liner adjusts the frequency where the most absorption will occur, with deeper liners corresponding to lower frequency absorption.

DDOF acoustic liners maintain the same design variables as the SDOF liner but includes an intermediate septum that introduces additional variables that can be altered to achieve higher acoustic absorbing performance. Like the facesheet in the SDOF, the DDOF facesheet also causes acoustic energy losses through friction within the perforations. This is added to by the perforations (porosity) in the intermediate septum. The lowest frequency response of the DDOF liner is still driven by the total depth, as with the SDOF, however the septum can cause additional ranges of high absorption. The core dividing septum has thickness, t_s , and variable permeability properties, such as percent open area, POA_s , and perforation diameter, d_s . The depth of the septum within the honeycomb core, D_s , can be varied as well, yielding in total three additional design variables. Figure 3b shows the honeycomb core liner with the additional septum related design variables included.

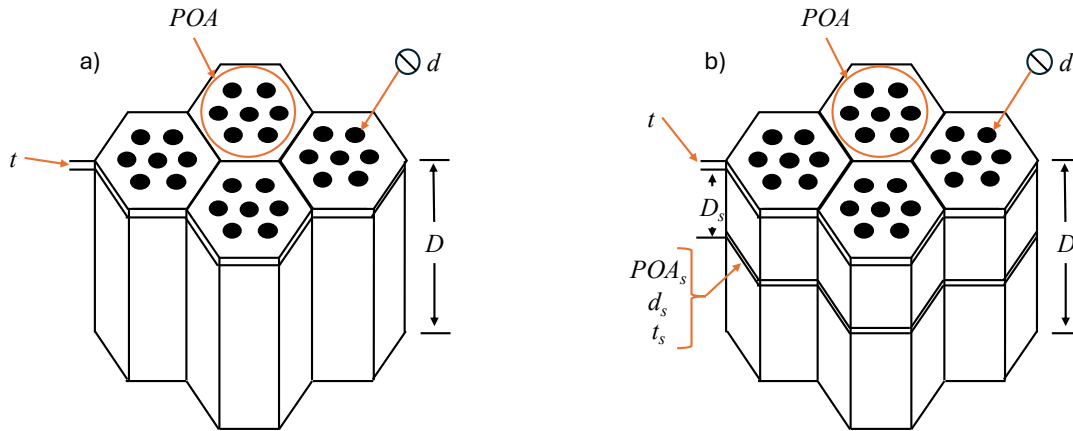


Figure 3. The SDOF and DDOF acoustic liners are shown. SDOF has four design variables: liner depth, D ; facesheet thickness, t ; facesheet perforation diameter, d ; percent open area, POA . The added septum in the DDOF creates four additional variables: septum depth, D_s , septum thickness, t_s , and percent open area and perforation diameter of the septum, POA_s and d_s .

3.1.2. TPMS

Instead of a cavity with variable depth, TPMS lattice structures encompass a complex pair of channels with unique tortuous paths that are controlled by specific design variables. The design variables used in this study are general to all TPMS lattices, but the lattice types of Schwarz P and Schwarz D (or Diamond) were selected for exploration and comparison with the SDOF and DDOF. Schwarz P was selected for the study based on the research team's previous preliminary investigations, while the Diamond lattice was selected for its high levels of internal tortuosity. The

first group of design variables is the variability of unit cell size. This allows us to adjust the size of individual unit cells in 3 directions, X , Y , and Z , effectively stretching or compressing the cells of the lattice in those directions (see Figure 4b for changes in Z and Figure 4c for changes in X and Y). These variables can also be scaled uniformly to vary the overall size of the unit cell. Due to the symmetry inherent in normal incidence impedance testing, the unit cell size in X and Y were coupled, and the samples were modeled in a $1 \times 1 \times n$ stack of cells. The total depth of the sample was determined by the height of the cells (Z) multiplied by another design variable, the total number of cells in the Z -direction. These design variables modify the internal volumes of the lattices, potentially causing variations in the resonating effects of the geometry.

Control of the levelset or iso-surface offset of TPMS lattices allows for the offsetting of material from the surface midplane to either side of the surface. Mathematically, a levelset is a collection of all of the points where an equation equals a given value. In TPMS lattices, the levelset value determines the slice of the lattice equation where the geometry is defined. Variations of the levelset value are shown in Figure 4d for both the Schwarz P and Diamond lattices. TPMS lattices split a region into two non-intersecting sub-regions. Changes in levelset varies the volumes of the two sub-regions, expanding one while contracting the other, promoting a unique acoustic response in each region. These two subregions can be broadly differentiated as the endo-region and the exo-region. In this study, levelset was defined twice: once at the facesheet and once at the backplate. This causes a functional grading effect of the levelset, where cells of the lattice in the Z -direction can have different levelset values.

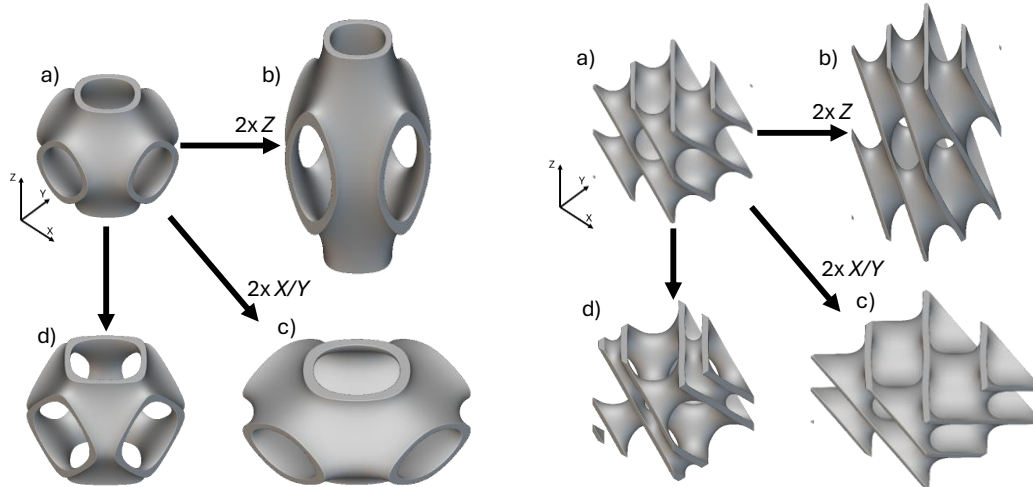


Figure 4. TPMS lattice variations from the basic unit cell (a) for the Schwarz P and Diamond lattices (left and right, respectively): change in Z height (b), change in X/Y width (c), change in levelset (d).

The additional benefit of the presence of the two sub-regions is that a unique facesheet can be applied to each region separately. In this way, each region essentially acts as its own acoustic liner, leading to the possibility of wider ranges of high acoustic absorption. For both the endo- and exo-regions, the design variables of perforation diameter and number of perforations can be defined uniquely. Examples of the facesheet over Schwarz P and Diamond unit cells are shown in Figure 5. The facesheet thickness is consistent between the two regions to avoid off-setting either

the top of the facesheet or the back of the lattice. This configuration leads to five design variables for the TPMS facesheet alone, in addition to the five variables from the lattice core geometry.

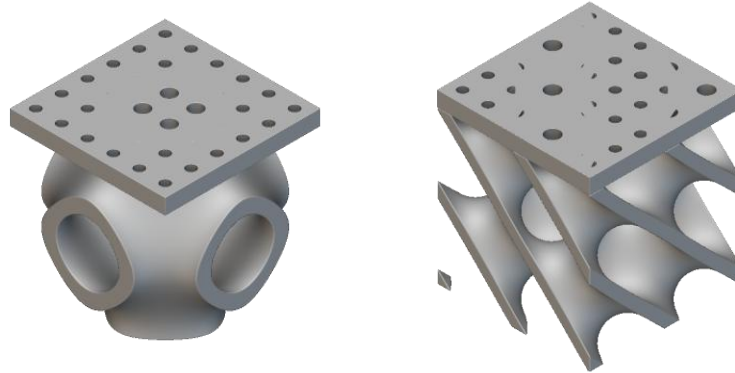


Figure 5. Facesheet depictions for the Schwarz P (left) and Diamond (right) TPMS lattice geometries. For these examples, the endo-region has a larger perforation diameter than the exo-region.

A summary of the available design variables associated with each liner in the current study is provided in Table 1. However, it is worth noting that the design complexity of TPMS lattices can be increased beyond the design variables implemented here. Additional variations can lead to structures with a graded wall thickness or volume fraction and hybrid lattices with two TPMS lattice types blending into one another. However, because the exact effect that the currently implemented variables have on acoustic performance is not well characterized, the study excluded the addition of further design modifications and design complexity.

Table 1. Design variables of the SDOF, DDOF, and TPMS acoustic liners

SDOF	DDOF	TPMS
# of Facesheet Perforations	# of Facesheet Perforations	X/Y Unit Cell Size
Perforation Diameter	Perforation Diameter	Z Unit Cell Size
Facesheet Thickness	Facesheet Thickness	Z: # of Cells
Liner Depth	Liner Depth	Levelset (Facesheet)
	# of Septum Perforations	Levelset (Backplate)
	Septum Perf. Diameter	Facesheet Thickness
	Septum Thickness	Endo Perf. Diameter
	Septum Depth	# of Endo Perforations
		Exo Perf. Diameter
		# of Exo Perforations

Compatible design variables were given the same constraints across all liner types. For all liners, the maximum depth of the liners was set at 38mm. The facesheet thickness was constrained between a minimum thickness of 0.6mm and a max of 2mm. The perforation diameter was also constrained between 0.6mm and 2mm. The facesheet thickness and perforation diameter constraints were maintained for the intermediate septum, in the case of the DDOF liner.

3.2. Geometry Modeling and Acoustic Simulation

The next step in the process is to represent the liner geometry in a way that we can parameterize the important geometric components and calculate the acoustic performance.

3.2.1. Analytical Approach

For the SDOF and DDOF acoustic liners, the Zwikker-Kosten Transmission Line (ZKTL) method was used to model geometry and predict acoustic performance. It is a Python implementation of the method, based on the workflow described in several publications [7,37]. In this method, each section of the liner is represented by a transmission matrix, including both cavities and perforated sheets. For modeling of the perforated sheets, the flow resistance is calculated using the lumped element model or two-parameter model [34], shown in Equation 1.

$$\zeta = \theta + i\chi = \theta_{lin} + \theta_{nonlin} + i\chi_{fs} \quad (1)$$

In this equation, ζ represents the impedance, θ represents the acoustic resistance (linear and nonlinear), and χ represents the acoustic reactance of the facesheet. It is referred to as the two-parameter model because it breaks the acoustic resistance into two terms: the linear and the nonlinear resistance. For a detailed description of the ZKTL model, with the two-parameter perforated boundary, see the work of Jones and Howerton [7]. For both analytical and numerical solutions, a sound pressure level (SPL) of 120 dB was used.

3.2.2. Numerical Approach

The tradeoff of exploring higher complexity geometries is that analytical solutions often do not exist that can adequately model all the physics present in these structures. Because of this, a numerical approach is necessary. First, the acoustic liner structure must be modeled in CAD software, then a mesh will be applied to the geometry, and a numerical simulation of the physics will be applied to the mesh.

For the TPMS acoustic liners, an implicit geometry CAD software, nTop [16], was used to generate the lattice geometries. As an implicit geometry software tool, nTop is able to model mathematically defined functions and efficiently represent and export the complex lattice geometry. The lattice geometry files from nTop were then imported into COMSOL Multiphysics [38]. Additionally, select SDOF and DDOF designs were modeled in CAD and simulated in COMSOL for verification of the previously discussed analytical approach. Geometry generation of liner designs was performed on local desktop machines, but COMSOL Multiphysics software was run on a cluster computing cloud service through the university.

COMSOL is a mid-fidelity simulation software with a robust library for acoustic modeling. The pressure acoustics setup in the COMSOL Acoustics module was used to apply the necessary boundary conditions for modeling acoustic performance. All walls in the model were treated as hard wall boundaries, and a perforated plate boundary condition representing a perforated facesheet was used to reduce the computation time caused by attempting to mesh such small features as the facesheet perforations. The facesheet design variables were imported into the study and applied to this boundary condition. A physics-defined mesh was used, which automatically adjusts the element size according to the physics being simulated. The acoustic response is solved across a prescribed frequency range of 300-3400Hz, which are the lower and upper bound of viable frequencies of available normal incidence tube (NIT) experimental testing. After the acoustic data is gathered, the response objectives are extracted for performance characterization.

3.3. Response Objectives

The two main pieces of information that are output from both numerical and analytical acoustic modeling are acoustic resistance, θ , and reactance, χ , which make up the complex acoustic impedance. For every tested frequency, these values describe the resistance to sound flow due to friction and heat, and to inertia of the medium, respectively. These two quantities can be used to calculate the acoustic absorption coefficient, α , which is the response objective used in the optimizations. Acoustic absorption coefficient is calculated as follows for normal incident plane-wave acoustics.

$$\alpha = \frac{4\theta}{(1 + \theta)^2 + \chi^2} \quad (2)$$

The acoustic absorption coefficient is an efficient performance metric, providing a value between zero (complete reflection) and one (complete absorption) for each frequency. When plotted, the result is an acoustic absorption curve (see Figure 6).

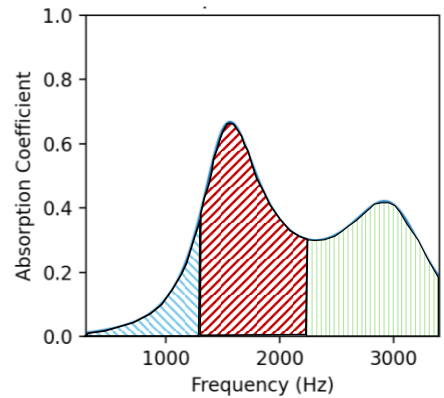


Figure 6. The acoustic absorption coefficient can be integrated over defined frequency bands to capture performance.

When calculating acoustic absorption for an acoustic liner design, the result is a series of absorption values for every frequency in the range that is tested. This poses difficulty when comparing the performance between two or more liners because it becomes inefficient to compare the absorption at every frequency. The most efficient metric would be a single scalar value to describe the general performance of the acoustic absorption coefficient in the desired frequency range. The method used to provide this metric is to integrate the absorption coefficient curve over -predetermined bandwidths (frequency ranges), yielding a single value describing the absorption performance. This can be done for both the entire sample bandwidth as well as smaller sub-bands. Figure 6 shows an example of the acoustic absorption coefficient and has indicated three regions, or sub-bands, across which the curve can be integrated. Where our simulations tested over a frequency range of 300-3400Hz, the absorption objectives of broadband (300-3400Hz), low band (300-1300Hz), mid band (1300-2300Hz), and high band (2300-3400Hz) were used in four distinct optimizations.

3.4. Optimization Approach

With design and simulation capabilities established and demonstrated, the optimization process was run through the design exploration and automation software, Altair HyperStudy, [43]. Hyperstudy was used as the interface for parameterizing the design variables of the liner

geometries and creating the design exploration routine. It was linked to nTop and was able to autonomously generate TPMS acoustic liner designs. However, due to the use of COMSOL being used on a remote server, direct automation between Hyperstudy and COMSOL was not available. Therefore, large, spacing-filling design of experiments (DOE) were established to generate many TPMS lattice geometries at once. Then, all the designs were uploaded to the COMSOL server where a batch script automation process was set up to iteratively simulate each design. When all designs were simulated, the acoustic results were imported back into Hyperstudy for analysis.

The traditional liners followed the same optimization approach as the TPMS designs, with the exception of the geometry and physics being modeled in a python script instead of nTop and COMSOL. Not needing the same computational power as the finite element solver, the ZKTL python script was run for the entire DOE on a local desktop machine, and results were imported immediately back into Hyperstudy. Verification using the COMSOL method was performed on select samples to ensure that the ZKTL code and initial search were providing usable results. The verification showed that the ZKTL script was accurate at low frequencies, but diverged slightly at higher frequencies, underpredicting the acoustic absorption. Because this underprediction was consistent across all samples, the ZKTL method was used to identify an estimation of acoustic performance, while COMSOL provided a higher fidelity solution and verification.

To identify the highest performing traditional and TPMS acoustic liner designs from their respective DOE datasets, a design exploration dashboard was created in HyperStudy, with tools to sort through the results. The HyperStudy dashboard is shown in Figure 7, with six panes that aid in the selection of high-performance acoustic liner designs. The TPMS lattice designs were sorted according to the four optimized frequency ranges, and the highest performing designs were identified.

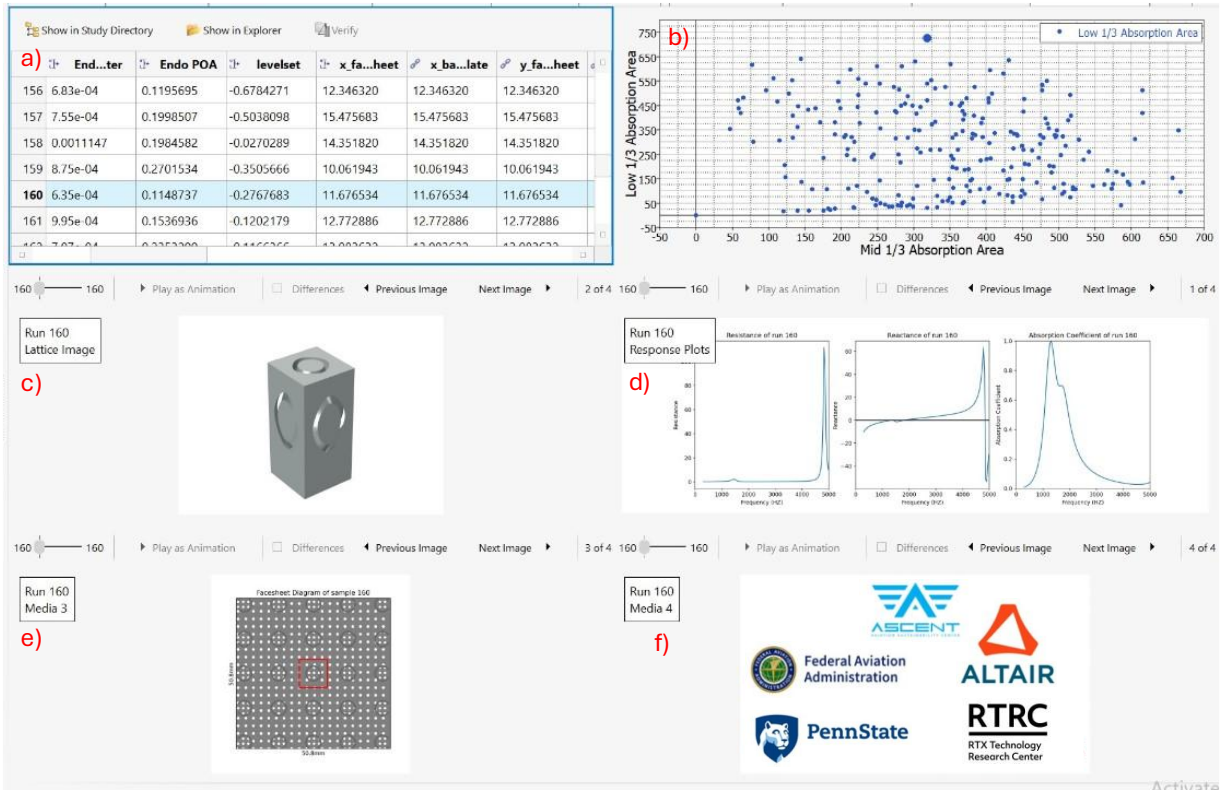


Figure 7. A design exploration dashboard was assembled in Altair HyperStudy with panes that show a) numerical design variable information for each sample, b) performance scatter plot that details the individual samples as points plotted by two selected response objectives; c) images depicting the lattice structure geometry d) acoustic impedance and absorption for individual selected sample, e) images depicting the geometry of the facesheet, and f) contributors logos.

4. Results and Discussion

Using the process outlined in Section 3, SDOF, DDOF, Schwarz P, and Diamond acoustic liners were optimized for acoustic absorption in four target frequency bandwidths: broadband (300-3400Hz), low band (300-1300Hz), mid band (1300-2300Hz), and high band (2300-3400Hz). DOE data sets were created for both TPMS-based liners, Schwarz P and Diamond, and traditional liners, SDOF and DDOF. 500 samples were generated for each TPMS-based liner and each traditional liner, from which the top performing designs would be selected for each lattice type. The simulation of each batch of lattice samples was done over the course of several days on the Penn State cluster computer due to the ~10 minute solution time for each sample. The ZKTL code for the traditional liners was much faster, solving all 500 samples in ~10 minutes on a local machine. Using the design exploration dashboard (Figure 7) the liner design concepts, with accompanying performance metrics, were sorted according to the response objectives of acoustic absorption over various frequency bandwidths. For each response objective and each liner type, the liner concept with the highest performance was identified.

For the traditional liners, after the highest performing liner designs were identified, they were modeled and simulated in COMSOL for verification. The coplotted ZKTL and COMSOL results are shown in Figure 8. The results of the two simulation methods predict similar trends in

the absorption coefficient curves, though at frequencies greater than 1600Hz, the COMSOL solution predicts higher absorption. This is less evident in the SDOF designs, which align very well in all cases except for the high band target. Because the COMSOL solution comes from a higher fidelity solver than the ZKTL solution, the comparisons with the TPMS liners were made using the COMSOL results. This also helps to ensure consistency within the analysis and optimization.

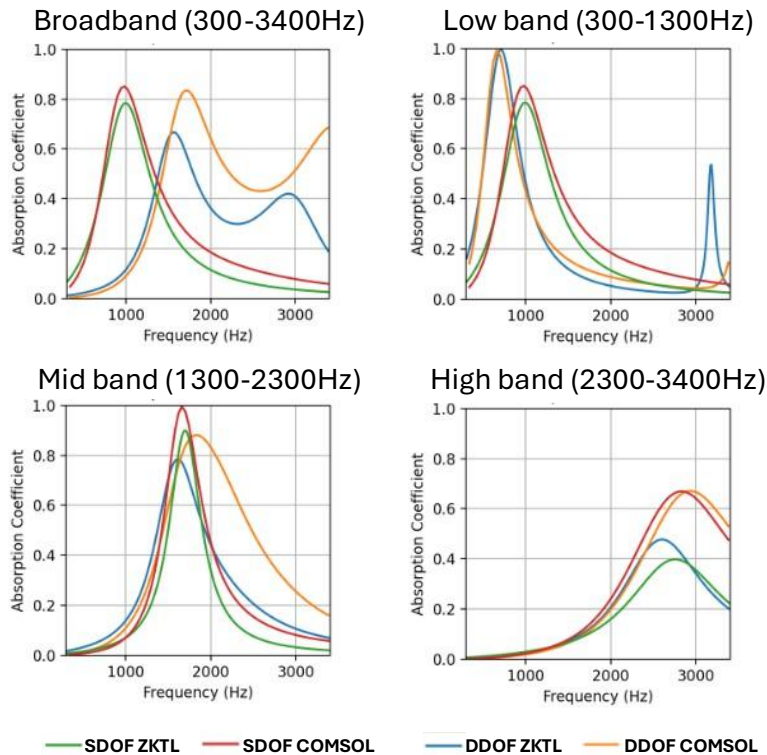


Figure 8. SDOF and DDOF samples compared using ZKTL and COMSOL solutions.

When looking at the images of the generated, optimized liner designs in the design exploration dashboard, trends were more easily noted in the SDOF and DDOF liner types than in the TPMS designs. For example, the trend for traditional liners total thickness (depth for the SDOF and the sum of two depths for the DDOF) led to deeper liners being better adapted to low frequencies and shorter liners being better adapted to high frequencies. However, a more nuanced assessment was revealed using a sensitivity analysis. The sensitivity analysis on the DOE results from the SDOF and DDOF liners showed that the facesheet variables, perforation diameter and the number of perforations, had some of the greatest impact across all target frequency bandwidths. Perforation diameter of the facesheet (as opposed to the septum) was consistently one of the most impactful design variables for the traditional liners. The facesheet was also highly impactful in the TPMS liner response, though the key design variable differed between the Diamond and Schwarz P. For the Diamond lattice, the number of perforations in both the endo and exo regions were highly impactful; the perforation diameters remained important, but X/Y unit cell size and number of stacked unit cells were more impactful across all target ranges. The two most impactful design variables for the Schwarz P liners were the exo region, facesheet perforation diameter, and number of perforations. This makes intuitive sense because the structure of the Schwarz P unit cell already

restricts the available open area of the endo region. For both Schwarz P and Diamond, in the high band target bandwidth, the number of stacked unit cells was the most impactful design variable. Because the number of cells directly influenced the total height of the liner, and high frequency absorption favors shorter channels, this design variable was critical for the high band regime.

With trends in the lattice geometry noted, the comparison results for liner performance are shown in Figure 9, where for each target frequency range, acoustic absorption coefficient is compared for the four liner types. In each of the target frequency bands, the TPMS acoustic liners had similar or better performance than the traditional liners; for example, in the broadband regime, the DDOF response value was 933Hz while the Schwarz P design had the value of 1372Hz. For the broadband target, SDOF peaked at a lower frequency than DDOF, Schwarz P, or Diamond; however, the absorption of the DDOF and TPMS designs acted across a wider frequency range, with the Schwarz P design showing the widest band. The low band target showed comparable results for all four liner types, all very high absorption coefficients at a peak frequency around 900Hz. The mid band target also showed a cluster where all liners peaked around 1850Hz, except the Schwarz P design also had an additional absorption peak at lower frequencies. Finally, in the high frequency target band, the TPMS designs showed higher absorption than the traditional liners.

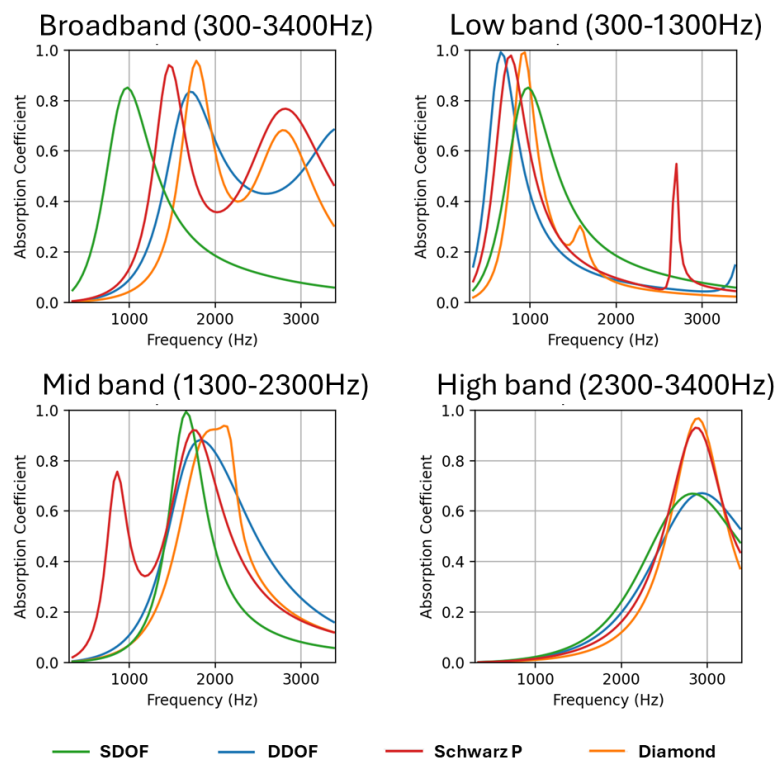


Figure 9. Acoustic absorption coefficient plots comparing four acoustic liner types, across four target frequency bands.

In the low, mid, and high band absorption objectives, the SDOF and DDOF acoustic liner types converged on designs that yielded similar performance. The intermediate perforated septum in the DDOF liner should produce a higher performance liner, however, all liners were subject to a maximum thickness constraint, which may have impeded the DDOF from taking full advantage of the perforated septum. Looking at the total depth of all the liners (displayed in Table 2), the

Schwarz P and Diamond acoustic liners required less height than the traditional liners to achieve competitive low and broadband acoustic absorption performance, as shown in **Table 2**. This suggests that using greater design freedom, such as with AM enabled TPMS lattice acoustic liners, performance of traditional acoustic liners can be matched, while requiring less volume within the nacelle. Additionally, there is a possibility for more attenuation to be achieved using liner depths associated with traditional designs. These are major findings for supporting the development of TPMS liners.

Table 2. Depth Across all Candidate Liner Types

Liner Type	Depth (mm)			
	Broadband	Low band	Mid band	High band
SDOF	36.0	36.0	7.3	11.0
DDOF	21.4	37.0	36.6	14.5
Schwarz P	11.9	27.1	16.0	12.5
Diamond	11.6	18.7	13.0	9.5

The absorption curves of the Diamond and Schwarz P liners show two peaks in all target ranges except the high band. In the broadband regime, the DDOF design mounts to what would be an additional peak, but that peak tip is out of the tested range. In the DDOF, the second peak is achieved through the perforated septum and the resonating effects of having two depths (from facesheet to septum, and from facesheet to backplate) creates two peaks. Due to the total depth constraint, the second peak is often out of the test range. For the TPMS lattices, propagation through the depth is potentially more tortuous. The second peak, in the case of these lattices, comes from the endo- and exo-regions. The facesheets over the two regions, in addition to differences in the internal channel, create an additional peak. Because the depth is constant, the second peak is largely controlled by the facesheet variables, so the two peaks are able to appear closer together. This is likely the cause of the mid band Diamond lattice behavior, where the peak plateaus before descending. This is a useful phenomenon when trying to absorb noise at two frequencies in close proximity with each other.

5. Conclusion and Future Work

Acoustic liners are required systems in modern aircraft engines to meet current aircraft and airport noise regulations. Driven by the need for higher performance acoustic structures, AM-enabled TPMS lattice structures have been explored for potential in acoustic applications. In this study, two types of TPMS lattice structures (Schwarz P and Diamond) were implemented in acoustic liner sandwich structure designs and acoustic absorption performance was compared with traditional SDOF and DDOF acoustic liners. After optimization with broadband, low, mid, and high band frequency range targets, it was found that the TPMS acoustic liners performance was equal to or greater than that of the optimized traditional acoustic liners. In the broadband and low frequency target comparisons, the TPMS liners achieved superior acoustic performance to the traditional liners while requiring significantly less overall liner thickness, further demonstrating the competitiveness of AM enabled TPMS lattices in acoustic liner applications.

With the wider set of design variables present for the more complex TPMS geometries, it becomes important to identify which factors are causing the acoustic effects shown in this study.

For example, linking the additional peaks of high absorption to the added complexity from design variables of the lattice, or the presence of two sets of facesheet variables atop two distinct volumes. This will be explored as future work building from this study, to identify the key design variables impacting absorption properties of TPMS-based acoustic liners. This will be accomplished through refinement of the DOE based on sensitivity analysis. An additional point of future work, and limitation of this study, involves the ZKTL model used to simulate the SDOF and DDOF acoustic liners. Some preliminary validation data has shown that the model is reliable at mid-low frequencies, but at higher frequencies produced some variation. This variation will be explored and improvements to the modeling process will be made.

Acknowledgement

This research was funded through the Pennsylvania State University Applied Research Laboratory's Walker Fellowship Program, the Office of Naval Research Naval Undersea Research Program (NURP, Contract #N000142312438) and the U.S. Federal Aviation Administration Office of Environment and Energy through ASCENT, the FAA Center of Excellence for Alternative Jet Fuels and the Environment, Project 79 through FAA Award Number 13-C-AJFE-PSU-113 under the supervision of Pierre Mulgrave. Any opinions, findings, conclusions or recommendations expressed in this material are those of the authors and do not necessarily reflect the views of the FAA.

References

- [1] M.G. Jones, W.R. Watson, D.M. Nark, B.M. Howerton, M.C. Brown, A Review of Acoustic Liner Experimental Characterization at NASA Langley, 2020. <http://www.sti.nasa.gov>.
- [2] J. Winkler, J.M. Mendoza, C.A. Reimann, K. Homma, J.S. Alonso, High fidelity modeling tools for engine liner design and screening of advanced concepts, *Int. J. Aeroacoustics* 20 (2021) 530–560. <https://doi.org/10.1177/1475472X211023884>.
- [3] M. Jones, D. Nark, Applications of Parallel-Element, Embedded Mesh-Cap Acoustic Liner Concepts, (n.d.). <https://ntrs.nasa.gov/api/citations/20190000891/downloads/20190000891.pdf> (accessed August 27, 2024).
- [4] M.G. Jones, F. Simon, R. Roncen, Broadband and Low-Frequency Acoustic Liner Investigations at NASA and ONERA, *AIAA J.* 60 (2022) 2481–2500. <https://doi.org/10.2514/1.J060862>.
- [5] J. Feng, J. Fu, X. Yao, Y. He, Triply periodic minimal surface (TPMS) porous structures: From multi-scale design, precise additive manufacturing to multidisciplinary applications, *Int. J. Extreme Manuf.* 4 (2022). <https://doi.org/10.1088/2631-7990/ac5be6>.
- [6] A.I. Komkin, M.A. Mironov, A.I. Bykov, Sound absorption by a Helmholtz resonator, *Acoust. Phys.* 63 (2017) 385–392. <https://doi.org/10.1134/S1063771017030071>.
- [7] M. Jones, B. Howerton, E. Ayle, Evaluation of Parallel-Element, Variable-Impedance, Broadband Acoustic Liner Concepts, in: 18th AIAACEAS Aeroacoustics Conf. 33rd AIAA Aeroacoustics Conf., American Institute of Aeronautics and Astronautics, Colorado Springs, CO, 2012. <https://doi.org/10.2514/6.2012-2194>.
- [8] M.B. Galles, M.G. Jones, D.M. Nark, An Initial Assessment of Variable Depth Liner Optimization for Ducted Proprotor Applications, in: 28th AIAACEAS Aeroacoustics 2022

- Conf., American Institute of Aeronautics and Astronautics, Southampton, UK, 2022. <https://doi.org/10.2514/6.2022-2821>.
- [9] A.T. Chambers, J.M. Manimala, M.G. Jones, Design and Optimization of 3D Folded-Core Acoustic Liners for Enhanced Low-Frequency Performance, *AIAA J.* 58 (2020) 206–218. <https://doi.org/10.2514/1.J058017>.
- [10] J.R. Kreitzman, M.G. Jones, Toward Fully 3D-Printed Two Degree of Freedom Acoustic Liners, in: *AIAA SCITECH 2024 Forum*, American Institute of Aeronautics and Astronautics, Orlando, FL, 2024. <https://doi.org/10.2514/6.2024-2801>.
- [11] H. Boden, S. Sack, S. Jacob, Impedance measurements for 3-D printed liners, in: *25th AIAACEAS Aeroacoustics Conf.*, American Institute of Aeronautics and Astronautics, Delft, The Netherlands, 2019. <https://doi.org/10.2514/6.2019-2600>.
- [12] G. Catapane, L.M. Cardone, G. Petrone, O. Robin, T. Humbert, K. Verdière, Labyrinth-Coiling Quarter Wavelength Tubes Embedded in Honeycomb Cells for Advanced Acoustic Liner Designs, in: *30th AIAACEAS Aeroacoustics Conf. 2024*, American Institute of Aeronautics and Astronautics, n.d. <https://doi.org/10.2514/6.2024-3251>.
- [13] X. Li, J.W. Chua, X. Yu, Z. Li, M. Zhao, Z. Wang, W. Zhai, 3D-Printed Lattice Structures for Sound Absorption: Current Progress, Mechanisms and Models, Structural-Property Relationships, and Future Outlook, *Adv. Sci.* 11 (2024) 2305232. <https://doi.org/10.1002/advs.202305232>.
- [14] K. Hur, R.G. Hennig, U. Wiesner, Exploring Periodic Bicontinuous Cubic Network Structures with Complete Phononic Bandgaps, *J. Phys. Chem. C* 121 (2017) 22347–22352. <https://doi.org/10.1021/acs.jpcc.7b07267>.
- [15] Z. Li, X. Li, Z. Wang, W. Zhai, Multifunctional sound-absorbing and mechanical metamaterials via a decoupled mechanism design approach, *Mater. Horiz.* 10 (2023) 75–87. <https://doi.org/10.1039/D2MH00977C>.
- [16] nTop, Release 4.10.2, nTop Inc., <https://ntop.com>, (n.d.).
- [17] J. Hu, S. Wang, Y. Wang, F. Li, Z. Luo, A lightweight methodology of 3D printed objects utilizing multi-scale porous structures, *Vis. Comput.* 35 (2019) 949–959. <https://doi.org/10.1007/s00371-019-01672-z>.
- [18] J. Fu, J. Ding, S. Qu, L. Zhang, M.Y. Wang, M.W. Fu, X. Song, Improved light-weighting potential of SS316L triply periodic minimal surface shell lattices by micro laser powder bed fusion, *Mater. Des.* 222 (2022) 111018. <https://doi.org/10.1016/j.matdes.2022.111018>.
- [19] Y. Lyu, T. Gong, T. He, H. Wang, M. Zhuravkov, Y. Xia, Study on the Energy Absorption Performance of Triply Periodic Minimal Surface (TPMS) Structures at Different Load-Bearing Angles, *Biomimetics* 9 (2024) 392. <https://doi.org/10.3390/biomimetics9070392>.
- [20] J. Iyer, T. Moore, D. Nguyen, P. Roy, J. Stolaroff, Heat transfer and pressure drop characteristics of heat exchangers based on triply periodic minimal and periodic nodal surfaces, *Appl. Therm. Eng.* 209 (2022) 118192. <https://doi.org/10.1016/j.applthermaleng.2022.118192>.
- [21] J. Wang, K. Chen, M. Zeng, T. Ma, Q. Wang, Z. Cheng, Investigation on flow and heat transfer in various channels based on triply periodic minimal surfaces (TPMS), *Energy Convers. Manag.* 283 (2023) 116955. <https://doi.org/10.1016/j.enconman.2023.116955>.
- [22] B.W. Reynolds, C.J. Fee, K.R. Morison, D.J. Holland, Characterisation of Heat Transfer within 3D Printed TPMS Heat Exchangers, *Int. J. Heat Mass Transf.* 212 (2023) 124264. <https://doi.org/10.1016/j.ijheatmasstransfer.2023.124264>.

- [23] G. Chouhan, B. Gunji, Additive manufacturing TPMS lattice structures: Experimental study on airflow resistivity, *Results Mater.* 20 (2023) 100478. <https://doi.org/10.1016/j.rinma.2023.100478>.
- [24] C. Lin, G. Wen, H. Yin, Z.-P. Wang, J. Liu, Y.M. Xie, Revealing the sound insulation capacities of TPMS sandwich panels, *J. Sound Vib.* 540 (2022) 117303. <https://doi.org/10.1016/j.jsv.2022.117303>.
- [25] S.H.N. Hoare, D.T. Murphy, Simulation of Acoustic Wave Propagation in 3-D Sonic Crystals based on Triply Periodic Minimal Surfaces, in: *Balt. Nord. Acoust. Meet. BNAM2012*, York, DNK, 2012. <https://eprints.whiterose.ac.uk/75127/> (accessed December 12, 2024).
- [26] Z. Li, X. Li, J.W. Chua, C.H. Lim, X. Yu, Z. Wang, W. Zhai, Architected lightweight, sound-absorbing, and mechanically efficient microlattice metamaterials by digital light processing 3D printing, *Virtual Phys. Prototyp.* 18 (2023) e2166851. <https://doi.org/10.1080/17452759.2023.2166851>.
- [27] N.V. Viet, N. Karathanasopoulos, W. Zaki, Mechanical attributes and wave propagation characteristics of TPMS lattice structures, *Mech. Mater.* 172 (2022) 104363. <https://doi.org/10.1016/j.mechmat.2022.104363>.
- [28] W. Elmadih, W.P. Syam, I. Maskery, D. Chronopoulos, R. Leach, Mechanical vibration bandgaps in surface-based lattices, *Addit. Manuf.* 25 (2019) 421–429. <https://doi.org/10.1016/j.addma.2018.11.011>.
- [29] W. Johnston, J. Godakawela, C. Gatti, S. Keshavanarayana, B. Sharma, Fibro-porous materials: 3D-printed hybrid porous materials for multifunctional applications, *Addit. Manuf.* 94 (2024) 104470. <https://doi.org/10.1016/j.addma.2024.104470>.
- [30] J. Godakawela, A. Lomte, B. Sharma, Sound absorption in uniform and layered gyroid and diamond triply periodic minimal surface porous absorbers, *Appl. Acoust.* 236 (2025) 110761. <https://doi.org/10.1016/j.apacoust.2025.110761>.
- [31] J. Godakawela, M. Carrillo-Munoz, B. Sharma, Enhancing the absorption performance of minimal surface-based bulk absorbers via symmetry-breaking, *INTER-NOISE NOISE-CON Congr. Conf. Proc.* 269 (2024) 837–844. https://doi.org/10.3397/NC_2024_0108.
- [32] N. Atalla, F. Sgard, Modeling of perforated plates and screens using rigid frame porous models, *J. Sound Vib.* 303 (2007) 195–208. <https://doi.org/10.1016/j.jsv.2007.01.012>.
- [33] N. Jiménez, J.-P. Groby, V. Romero-García, The Transfer Matrix Method in Acoustics, in: N. Jiménez, O. Umnova, J.-P. Groby (Eds.), *Acoust. Waves Period. Struct. Metamaterials Porous Media Fundam. Ind. Appl.*, Springer International Publishing, Cham, 2021: pp. 103–164. https://doi.org/10.1007/978-3-030-84300-7_4.
- [34] B.S. Beck, N.H. Schiller, M.G. Jones, Impedance assessment of a dual-resonance acoustic liner, *Appl. Acoust.* 93 (2015) 15–22. <https://doi.org/10.1016/j.apacoust.2015.01.011>.
- [35] TRANSFER-MATRIX SOLUTIONS, n.d.
- [36] M.G. Jones, T.L. Parrott, W.R. Watson, Uncertainty and Sensitivity Analyses of a Two-Parameter Impedance Prediction Model, n.d.
- [37] T.L. Parrott, M.G. Jones, Parallel-element liner impedances for improved absorption of broadband sound in ducts, *Noise Control Eng. J.* 43 (1995) 183–195. <https://doi.org/10.3397/1.2828379>.
- [38] COMSOL Multiphysics v. 6.2. www.comsol.com. COMSOL AB, Stockholm, Sweden, (n.d.).

- [39] N.H. Schiller, M.G. Jones, B. Bertolucci, Experimental Evaluation of Acoustic Engine Liner Models Developed with COMSOL Multiphysics, n.d.
- [40] A. Mann, F. Pérot, M.-S. Kim, D. Casalino, Characterization of Acoustic Liners Absorption using a Lattice-Boltzmann Method, (n.d.). <https://doi.org/10.2514/6.2013-2271>.
- [41] F. Avallone, P. Manjunath, D. Ragni, D. Casalino, Lattice-Boltzmann Very Large Eddy Simulation of a Multi-Orifice Acoustic Liner with Turbulent Grazing Flow, in: 25th AIAACEAS Aeroacoustics Conf., American Institute of Aeronautics and Astronautics, 2019. <https://doi.org/10.2514/6.2019-2542>.
- [42] P. Manjunath, F. Avallone, D. Casalino, D. Ragni, M. Snellen, Characterization of Liners using a Lattice-Boltzmann Solver, in: 2018 AIAACEAS Aeroacoustics Conf., American Institute of Aeronautics and Astronautics, 2018. <https://doi.org/10.2514/6.2018-4192>.
- [43] Altair Hyperstudy, v. 2022.3, Altair Engineering Inc., <https://altair.com/hyperstudy>, (n.d.).